Sensors & Transducers, Vol. 225, Issue 9, September 2018, pp. 19-24

www.sensorsportal.com

Sensors & Transducers

Published by IFSA Publishing, S. L., 2018
http://www.sensorsportal.com

Preparation of an Organic Waveguide Electro-optic Modulator Operating in the Visible Spectral Range

*** Edgars NITISS, Janis BUSENBERGS, Andrejs TOKMAKOVS and Martins RUTKIS**

Institute of Solid State Physics, University of Latvia, Kengaraga 8, Riga, Latvia, LV-1063
Tel.: +371 67260787
E-mail: edgarsn@cfi.lu.lv

Received: 25 June 2018 /Accepted: 31 August 2018 /Published: 30 September 2018

Abstract: In this contribution we demonstrate an all-organic Mach-Zehnder interferometric electro-optic waveguide modulator capable of operating in the visible and infrared spectral range. We demonstrate experimentally an operation of modulator design that comprises SU-8 as waveguide core and an electro-optic host-guest glass forming polymer as a cladding. The modulator is tested in the visible part of the spectral range and the results indicated comparatively high efficiency in-device in-plane poling (up to 30 %) of the value reached in thin films.

Keywords: Integrated optics devices, Modulators, Electro-optic polymer, Waveguide Mach-Zehnder.

1. Introduction

One of the central problems in the field of photonics research and industry has been the realization of high-bandwidth and small footprint electro-optic (EO) devices for applications in high-speed communication and computing. Organic materials have shown to be potential candidates to be used in these devices as the nonlinear optical (NLO) medium due to multiple of their advantageous properties such as low cost, low dielectric constants and high EO coefficients (>300 pm/V) [1]. Very recently a significant breakthrough has been achieved in the field through improvement of EO materials and demonstration of novel hybrid silicon-organic and plasmonic-organic device architectures [2–5]. Despite these achievements there still is an ongoing pursue of organic EO materials and modulator designs that could meet the requirements for their widespread commercial utilization. Here we present our efforts and results in preparation of an all-organic Mach-Zehnder interferometric (MZI) EO waveguide modulator capable of operating in the visible and infrared spectral range.

2. Design and Fabrication

The MZI waveguide device was fabricated on a glass substrate. Two optical lithography steps were performed using a 365 nm laser writer μPG 101. In the first step electrode mask was made in a positive tone resist MEGAPOSIT SPR 700 and 100 nm thick Chromium electrodes were sputtered using thermal evaporator (Edwards). In the second step direct writing of MZI waveguide structure was carried out in SU-8 negative resist. The SU-8 is an epoxy-based negative photoresist with low absorption coefficients in the visible and infrared spectra, a high glass-transition temperature and good chemical durability. The SU-8 resist was prepared by spin-coating technique. The required thickness was achieved by

diluting GM-1075 SU-8 negative-tone photo-epoxy from Gerseltec in gamma-Butyrolactone (GBL) as well as by varying the spin-coating speed. Below in Fig. 1 the thickness dependence on both mentioned parameters is shown.

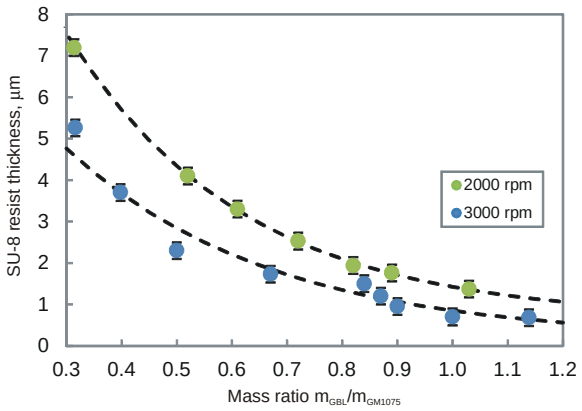

Fig. 1. Thickness of SU-8 resist coated at two spin-coating speeds – 2000 and 3000 rpm – as a function of mass ratio of diluent GBL and GM-1075 SU-8 negative tone photo-epoxy.

The top and side views of modulator design are as depicted in Fig. 2. It comprises an SU-8 waveguide core, electrodes in the plane with the waveguide core and an EO polymer coating and its operation and optimization principles have been profoundly described elsewhere [6-7].

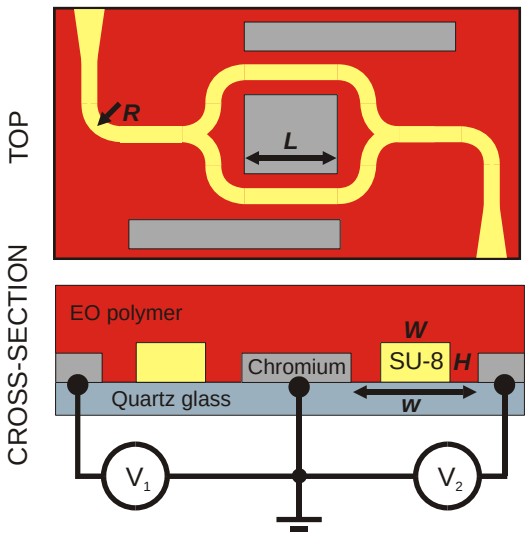

Fig. 2. The top-view and cross-section of the waveguide MZI. Here R is the waveguide bend radius, L is the central electrode and interaction length, w is the electrode separation length, W and H are the SU-8 waveguide core width and height respectively. Voltages V_1 and V_2 can be applied during poling and modulation.

The waveguide MZI was purposely made asymmetric such that the light interference had a phase bias of $\pi/2$. The structure was then spin-coated with a host-guest polymer comprising 2-(4-(bis(5,5,5-triphenylpentyl)amino) benzylidene)-1H-indene-1,3(2H)-dione (DMABI-Ph6) as NLO chromophore and PMMA as matrix. The second and third order NLO properties of DMABI-Ph6 have been described elsewhere [8-9].

DMABI-Ph6 was selected mainly due to three reasons. Firstly, DMABI-Ph6 is an organic glass and therefore is amorphous and would not crystallize during poling. Secondly, DMABI-Ph6 possesses high NLO efficiency as measured by Maker fringe technique at 1064 nm using setup described elsewhere [10]. Corona poled DMABI-Ph6 thin films had an NLO coefficient of $d_{33}(532)=69.2$ pm/V. Yet it is important to note that the NLO coefficient values are resonantly enhanced due to the fact that the second harmonic of 1064 nm is in the absorption band of the material. Using relations described by Oudar and Chemla [11] as well as by Singer [12], we estimated that the EO coefficient r_{33} of pure DMABI-Ph6 at 633 nm should maximally be around 3 pm/V.

Thirdly, the refractive index of thin films made of DMABI-Ph6 can be varied by changing the NLO chromophore concentration in a PMMA matrix. Below in Fig. 3 we show the refractive index of guest-host films made of DMABI-Ph6 in PMMA as well as the measured refractive index of SU-8. The concentration C of DMABI-Ph6 in the PMMA matrix expressed as

$$C = \frac{m_{DMABI-Ph6}}{m_{DMABI-Ph6} + m_{PMMA}}, \quad (1)$$

where $m_{DMABI-Ph6}$ is the mass of the chromophore and m_{PMMA} is the mass of PMMA.

Since the SU-8 will is used as a waveguide core, the employed cladding should have a refractive index that is lower than that of cladding. As evident from Fig. 3 the DMABI-Ph6 concentration in PMMA should not exceed the concentration value of 40 % wt.

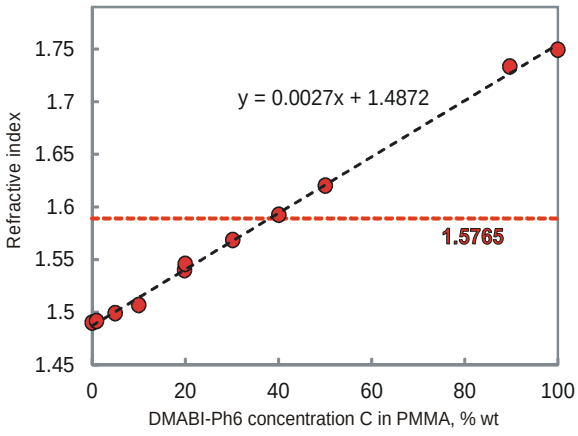

Fig. 3. The refractive index of guest-host DMABI-Ph6 + PMMA films measured at 633 nm by prism-coupling technique as a function of NLO chromophore concentration is indicated by red circles. The red dotted line indicates the refractive index of SU-8 at 633 nm.

We calculated the operation conditions of the waveguide MZI at different NLO polymer cladding refractive indexes. We used finite element mode solver in Comsol Multiphysics 5.2a Wave Optics module to calculate the effective refractive indexes n_{eff} of the first two modes as well as the overlap integral Γ of the first mode at 633 nm in the waveguide at different DMABI-Ph6 chromophore concentrations. The overlap integral Γ describes the interaction efficiency between the applied electric field and the optical mode [13]. The calculated n_{eff} and Γ values are depicted Fig. 4. The desired single mode regime is restricted by the black dotted lines, which are located at 27 % wt and 38 % wt, respectively.

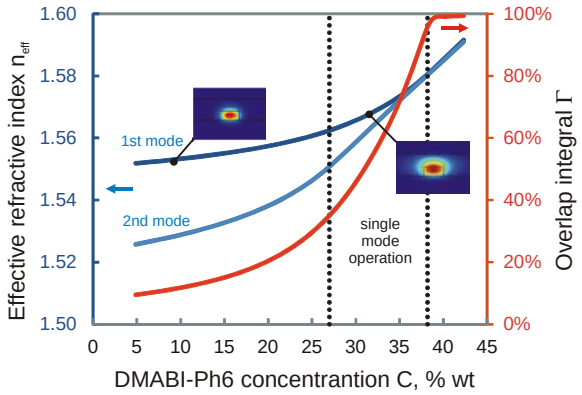

Fig. 4. The effective refractive index n_{eff} of first and second TE modes as a function of DMABI-Ph6 concentration in PMMA matrix are plotted with blue lines on primary y axis. The overlap integral Γ of the 1st mode is plotted with the red line on secondary y axis. The dotted vertical line indicates concentration at which the waveguide operates in single mode regime.

It is important to understand other properties of the material when chromophore concentration is varied. Parameters such as glass transition temperature and NLO coefficients are important in the device preparation process as well as testing. We used second harmonic generation intensity decay measurements to estimate the glass transition temperature as well as NLO coefficients of films prepared at different chromophore concentration C. Firstly we found that by adding chromophores to PMMA significantly reduces the glass transition temperature of the material. The glass transition temperature drops and saturates at around 77°C at by adding as little as 10 % wt of DMABI-Ph6 in PMMA matrix. As expected the observable macroscopic nonlinearity of the film reduced by decreasing the chromophore concentration in the material. The measured NLO coefficient d_{33} at zero frequency of pure DMABI-Ph6 poled by Corona poling method was 6.29 pm/V, while at 30 % wt dropped to around 1 pm/V. From this value the estimated EO coefficient was around 0.65 pm/V. It is important to note that we did not observe a drop in the optical nonlinearity at higher chromophore concentrations. This suggests that there is weak dipole-dipole interaction between chromophores in the film.

The concentration of chromophore in the matrix was chosen to be 30 % wt. At this concentration the refractive index of EO polymer is such that a single mode condition is met if other parameters of the device are as shown in Table 1.

Table 1. The created EO device and employed material parameters.

Parameter	Value
Substrate refractive index at 633 nm	1.45
SU-8 refractive index at 633 nm	1.589
EO polymer refractive index at 633 nm	1.5684
SU-8 core width	1.5 μm
SU-8 core height	0.7 μm
Waveguide bend radius	0.5 mm
EO cladding thickness	1 μm
Interaction length	5 mm
Electrode height	100 nm
Electrode separation distance	20 μm
Estimated overlap integral Γ	50 %
NLO coefficient at 532 nm	69.2 pm/V
NLO coefficient at zero frequency	6.29 pm/V
Estimated EO coefficient at 633 nm	0.65 pm/V

An important part in the device preparation is the polymer poling. Poling is a process in which the NLO chromophores are aligned non-centrosymetrically. For maximal possible NLO efficiency one must achieve the highest polar order of chromophore molecules in the matric while maintaining the chromophore structure, concentration and good optical properties of the cladding. Typically thin films are poled by Corona poling method which has shown to be one of the most efficient polymer poling methods due to many of its advantages [14]. Unfortunately, Corona poling cannot be applied for poling the NLO polymer employed in the device described here and in-device poling method will have to be applied.

For poling and EO modulation purposes the electrical wires were connected to Chromium electrodes by Silver paste. The poling was done at temperature that was 20°C above the glass transition temperature of EO polymer with poling field of 40 V/μm. This procedure was done on a temperature stabilized hot-plate by setting the poling voltage and capturing poling currents with a 6517B electrometer (Keithley). To our observation, increase of either the poling temperature or field above the mentioned above would result dielectric breakdown which makes the device unusable.

We initially prepared the device on a regular soda lime glass. During the poling procedure we noticed morphology changes in the electrodes. Moreover, the electrode that was connected to the ground during poling became non-conducting. Below in Fig. 5 the optical images of Chromium electrodes after applying 190 V and heating the substrate to 105°C are shown.

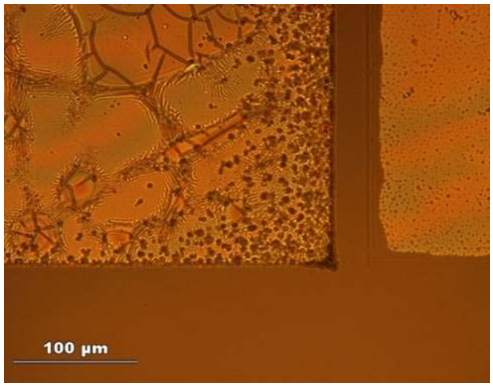

Fig. 5. Optical image of electrodes on soda lime glass after applying 190 V and heating the substrate to 105°C. The electrodes are separated by 30 µm. The left electrode was connected to ground during poling.

The X-ray photoelectron spectroscopy (XPS) depth profiling measurements on the electrodes were performed after poling showing that the temperature and electric field induced ion diffusion is the cause of electrode morphology change. Below in Fig. 6 the atomic percentage of Chromium and Sodium as a function of surface etch time is shown. The etch time correlates linearly with the etched depth. As evident from Fig. 6, during poling the Chromium has diffused inward the substrate while Sodium ions have diffused outward.

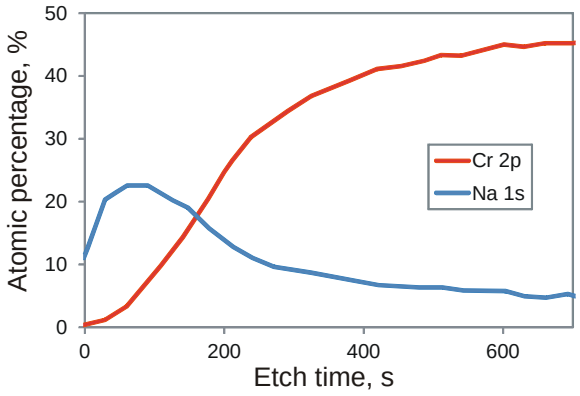

Fig. 6. XPS measurements – atomic percentage of Chromium and Sodium as a function of surface etch time which is proportional to depth.

In order to avoid morphology changes in the electrodes the device was prepared on a quartz glass substrate which has lower conductivity than soda lime glass by around three orders of magnitude. Below in Fig. 7 Optical image of electrodes on quartz glass after applying 190 V and heating the substrate to 105°C is shown. As evident, the electrodes have not changed during poling.

After NLO polymer poling within devices, the lower side of the substrate was slightly cut using a diamond saw thus allowing fine breaking of the substrate and the waveguides. The light could be coupled into the waveguide through the facet (see Fig. 2) without any additional polishing or preparation steps.

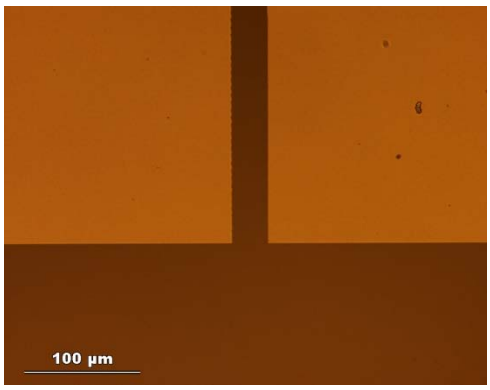

Fig. 7. Optical image of electrodes on quartz glass after applying 190 V and heating the substrate to 105°C. The electrodes are separated by 30 µm.

3. Characterization

The setup used for testing the EO modulator is shown in Fig. 5. Here we used a 2 mW He-Ne laser operating at 633 nm as light source for exciting the TE mode in the waveguide. The laser beam was coupled to the MZI and collected via 20x microscope objectives. Below in Fig. 8 an optical image from the top of waveguide MZI with excited guiding mode is displayed. In the same figure the electrical wires connected to Chromium electrodes by Silver paste are evident. Due to partly destructive interference at the second waveguide splitter part of the energy is being scattered in form of radiation modes. Unfortunately, due to poor dynamic range of the camera this scattering is not pronounced however is visible by eye in the microscope.

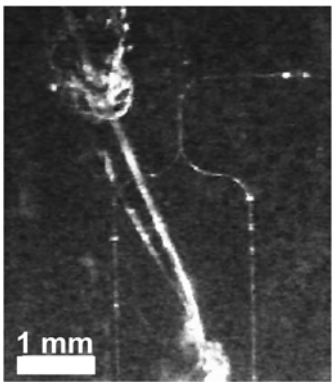

Fig. 8. An optical image from the top of waveguide MZI with excited guiding mode.

We used a function generator, phase inverter and a dual-channel amplifier for applying the modulating

voltage in a push-pull regime. The light intensity modulations were recorded using a high speed silicon photodetector connected to an oscilloscope.

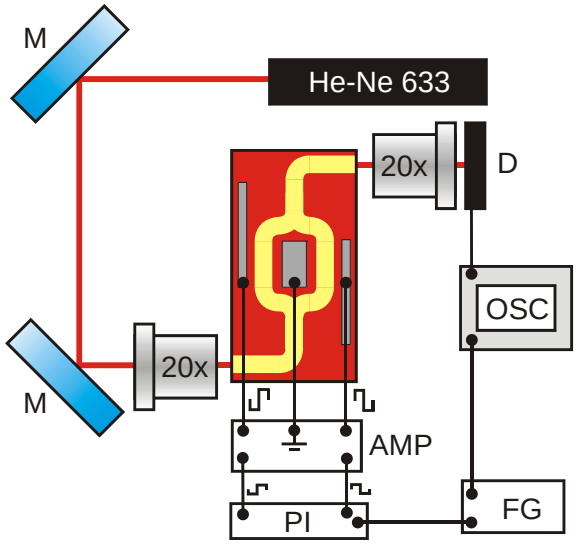

Fig. 9. The setup for electro-optic characterization of the device: He-Ne 633 – laser, M – mirrors, D – detector DET36A (Thorlabs), OSC – oscilloscope, FG – function generator, PI – phase inverter, and AMP – amplifier.

In Fig. 10 the applied modulation field and captured modulated signal are shown. As evident from Fig. 10 the modulation bandwidth is low. By fitting the decay of intensity we estimate the bandwidth to be at around 4 kHz. The main cause of such low bandwidth is the contact resistance of the Silver paste (~1 kOhm) as well the high wire capacitance (~0.2 nF). The RC time constant estimated from these values agrees well with the experimentally observed modulation bandwidth.

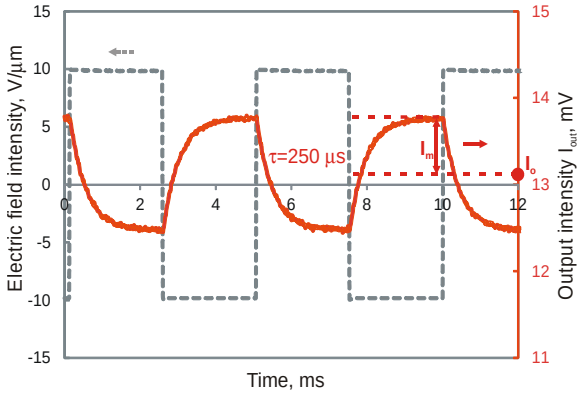

Fig. 10. The applied modulating field intensity and the output light intensity as a function of time.

For estimation of effective EO coefficient r from the modulation data we used the following approximation:

$$r = \frac{I_m}{I_o} \frac{\lambda}{\pi \cdot n^3 \cdot E \cdot L \cdot \Gamma}, \qquad (2)$$

where I_m is the light intensity modulation amplitude, I_o is the average light output intensity, λ is the wavelength, n is the EO polymer refractive index, E – the applied modulating field, L – interaction length, Γ – the overlap integral. From eq. (2) we get that EO coefficient r=0.20 pm/V which is approximately 30% of the value estimated from the NLO measurement in thin film poled by Corona poling method.

4. Conclusions

We have successfully demonstrated engineering, development and the operation of an all-organic EO modulator. The efficiency of the device is very poor which is due to low EO coefficients of employed polymer. It is recognized that the drive voltage at TTL level of 5 V could be reached if the current state-of-the-art organic EO materials with EO coefficient >100 pm/V would be used in the device.

Acknowledgements

Use the Acknowledgements section if it is necessary. This work was supported by ERDF 1.1.1.1 activity project Nr. 1.1.1.1/16/A/046 “Application assessment of novel organic materials by prototyping of photonic devices”.

References

[1]. L. R. Dalton, D. Lao, B. C. Olbricht, S. Benight, D. H. Bale, J. A. Davies, T. Ewy, S. R. Hammond, P. A. Sullivan, Theory-inspired development of new nonlinear optical materials and their integration into silicon photonic circuits and devices, *Optical Materials*, Vol. 32, Issue 6, 2010, pp. 658–668.

[2]. W. Heni, C. Haffner, D. L. Elder, A. F. Tillack, Y. Fedoryshyn, R. Cottier, Y. Salamin, C. Hoessbacher, U. Koch, B. Cheng, B. Robinson, L. R. Dalton, J. Leuthold, Nonlinearities of organic electro-optic materials in nanoscale slots and implications for the optimum modulator design, *Optics Express*, Vol. 25, Issue 3, 2017, pp. 2627–2653.

[3]. S. Koeber, R. Palmer, M. Lauermann, W. Heni, D. L. Elder, D. Korn, M. Woessner, L. Alloatti, S. Koenig, P. C. Schindler, H. Yu, W. Bogaerts, L. R. Dalton, W. Freude, J. Leuthold, C. Koos, Femtojoule electro-optic modulation using a silicon–organic hybrid device, *Light: Science & Applications*, Vol. 4, Issue 2, 2015, e255.

[4]. C. Hoessbacher, A. Josten, B. Baeuerle, Y. Fedoryshyn, H. Hettrich, Y. Salamin, W. Heni, C. Haffner, C. Kaiser, R. Schmid, D. L. Elder, D. Hillerkuss, M. Möller, L. R. Dalton, J. Leuthold, Plasmonic modulator with >170 GHz bandwidth demonstrated at 100 GBd NRZ, *Optics Express*, Vol. 25, Issue 3, 2017, pp. 1762–1768.

[5]. Y. Shi, W. Lin, D. J. Olson, J. H. Bechtel, H. Zhang, W. H. Steier, C. Zhang, L. R. Dalton, Electro-optic polymer modulators with 0.8 V half-wave voltage, *Applied Physics Letters*, Vol. 77, Issue 1, 2000, pp. 1–3.

[6]. E. Nitiss, Evaluation of performance of a hybrid electro-optic directional coupler and a Mach–Zehnder switch, *Journal of Nanophotonics*, Vol. 11, Issue 1, 2017, 16013.

[7]. E. Nitiss, A. Tokmakovs, K. Pudzs, J. Busenbergs, M. Rutkis, An electro-optic organic waveguide modulator operating in the visible spectral range, in *Proceedings of the 1st International Conference on Optics Photonics and Lasers (OPAL'2018)*, Barcelona, Spain, 9-11 May 2018, pp. 145-148.

[8]. E. Nitiss, A. Tokmakovs, K. Pudzs, J. Busenbergs, M. Rutkis, All-organic electro-optic waveguide modulator comprising SU-8 and nonlinear optical polymer, *Optics Express*, Vol. 25, Issue 25, 2017, pp. 31036-31044.

[9]. A. Bundulis, E. Nitiss, M. Rutkis, Determination of Kerr and two-photon absorption coefficients of ABI thin films, in *Proceedings of SPIE on Nonlinear Optics and its Applications at SPIE Photonics Europe*, Strasbourg, France, 22-26 April 2018, 10684-81.

[10]. M. Rutkis, A. Vembris, V. Zauls, A. Tokmakovs, E. Fonavs, A. Jurgis, V. Kampars, Novel second-order non-linear optical polymer materials containing indandione derivativatives as a chromophore, in *Proceedings of SPIE on Organic Optoelectronics and Photonics II at SPIE Photonics Europe*, Strasbourg, France, 3 - 7 April 2006, 61922Q–8.

[11]. J. L. Oudar, D. S. Chemla, Hyperpolarizabilities of the nitroanilines and their relations to the excited state dipole moment, *Journal of Chemical Physics*, Vol. 66, Issue 6, 1977, pp. 2664–2668.

[12]. K. D. Singer, M. G. Kuzyk, J. E. Sohn, Second-order nonlinear-optical processes in orientationally ordered materials: relationship between molecular and macroscopic properties, *Journal of the Optical Society of America B*, Vol. 4, Issue 6, 1987, pp. 968–976.

[13]. R. C. Alferness, Waveguide Electrooptic Modulators, *IEEE Transactions on Microwave Theory and Techniques*, Vol. 30, Issue 8, 1982, pp. 1121–1137.

[14]. E. Nitiss, E. Titavs, K. Kundzins, A. Dementjev, V. Gulbinas, M. Rutkis, Poling induced mass transport in thin polymer films, *Journal of Physical Chemistry B*, Vol. 117, Issue 9, 2013, pp. 2812–2819.